ACS NANO

www.acsnano.org

ARTICLE

Multiscale Self-Assembly of Distinctive Weblike Structures from Evaporated Drops of Dilute American Whiskeys

Adam D. Carrithers,[§] Martin J. Brown, VI,[§] Mohamed Z. Rashed, Sabina Islam, Orlin D. Velev, and Stuart J. Williams*

Cite This: https://dx.doi.org/10.1021/acsnano.9b08984

Read Online

ACCESS | Metrics & More | Article Recommendations | Supporting Information

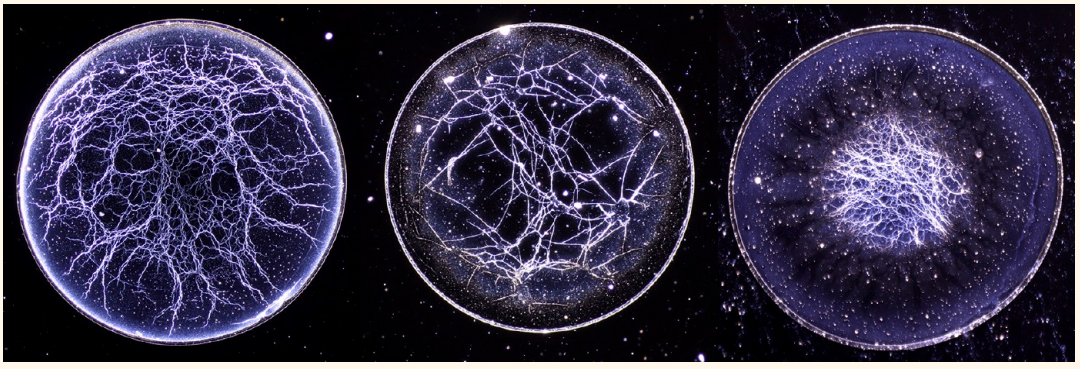

ABSTRACT: When a sessile droplet of a complex mixture evaporates, its nonvolatile components may deposit into various patterns. One such phenomena, the coffee ring effect, has been a topic of interest for several decades. Here, we identify what we believe to be a fascinating phenomenon of droplet pattern deposition for another well-known beverage—what we have termed a "whiskey web". Nanoscale agglomerates were generated in diluted American whiskeys (20−25% alcohol by volume), which later stratified as microwebs on the liquid−air interface during evaporation. The web's strandlike features result from monolayer collapse, and the resulting pattern is a function of the intrinsic molecular constituents of the whiskey. Data suggest that, for our conditions (diluted 1.0 μL drops evaporated on cleaned glass substrates), whiskey webs were unique to diluted American whiskey; however, similar structures were generated with other whiskeys under different conditions. Further, each product forms their own distinct pattern, demonstrating that this phenomenon could be used for sample analysis and counterfeit identification.

KEYWORDS: *self-assembly, colloids, surface monolayers, Marangoni flow, droplet evaporation, whiskey*

An evaporating droplet containing nonvolatile solutes leaves a deposit whose form is dependent on the intrinsic properties of the liquid,[1,2] the nature of the solutes or particles,[3,4] and the environmental conditions under which evaporation takes place.[5,6] Understanding the deposition of such nonvolatile solutes is critical for engineering of coating and patterning processes.[7] One common phenomenon, which can arise in these coating processes, is the coffee ring deposition effect where solute particles are transported to the pinned contact line *via* capillary flow.[8] Suppression of the coffee ring effect has been extensively studied with various liquids,[9] including Scotch whiskey, which yielded nearly uniform particle deposition.[10]

Here, we demonstrate a self-assembled structure resulting from the evaporation of a volatile sessile drop of American whiskeys—depositing hierarchical weblike patterns that we have termed a "whiskey web".[11] These webbed patterns were formed by evaporating a 1.0 μL droplet of diluted American whiskey onto a clean glass coverslip. Results herein will

Received: November 12, 2019
Accepted: March 9, 2020

https://dx.doi.org/10.1021/acsnano.9b08984
ACS Nano XXXX, XXX, XXX−XXX

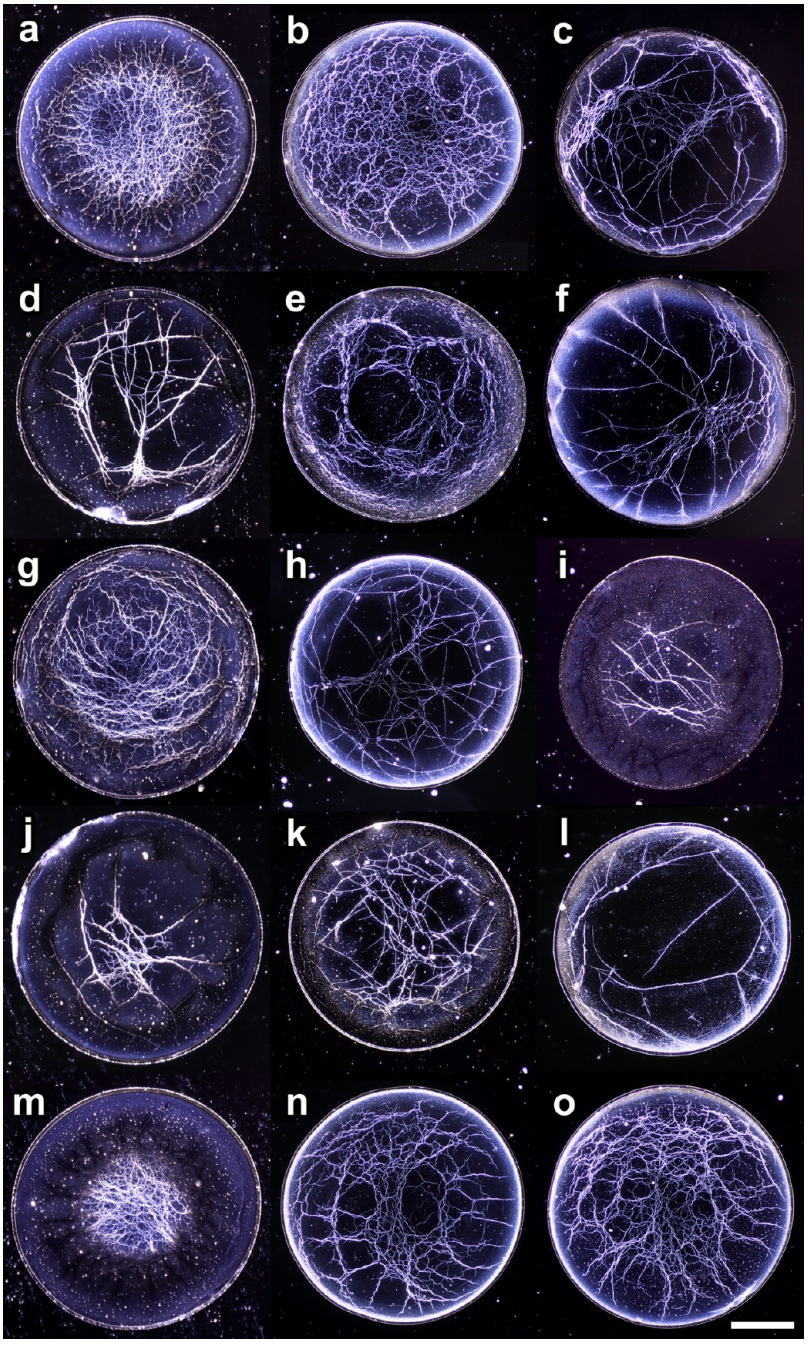

Figure 1. Examples of the surprisingly diverse "whiskey web" patterns. The patterns, approximately 2 mm in diameter, were formed by drying droplets from various off-the-shelf whiskey products diluted to 20−25% alcohol by volume. Scale bar is 0.5 mm. Refer to Table S1 in the Supporting Information for sample identification. Adapted with permission under a Creative Commons Attribution-NonCommercial 4.0 International License from ref 11, https://doi.org/10.1103/APS.DFD.2018.GFM.P0002. Copyright 2018 Stuart J. Williams.

demonstrate that these weblike structures are monolayers of water-insoluble chemical constituents that collapsed at the interface of the sessile droplet. Traditionally, Langmuir monolayers have been studied to gain insight into the behavior of biological membranes,[12] to develop thin films,[13] or to understand structural and phase transitions.[14−16] Inadvertently, this work demonstrated not only that such structures are created during droplet evaporation, as one might expect for the analogous monolayer compression experiment,[17−19] but also that the resulting pattern serves as chemical "fingerprints" of the liquid. Figure 1 shows a selection of qualitatively repeatable patterns generated from evaporated 1.0 μL drops of diluted (20−25% alcohol by volume) American whiskey deposited on coverslip glass.

The chemical composition of the whiskeys has an obvious impact on monolayer composition and connectivity, thus resulting in different patterns. The folds themselves can resemble "twisted ribbons", and in certain cases, monolayer collapse leads to the formation of vesicles.[14,20] The collapse of the monolayers is further influenced by interfacial intermolecular interactions, including alkyl chain length, headgroup ionization, strength of interfacial hydrogen bonding, temperature, and compression rate.[21] Its heterogeneity, including contaminants, plays a role in the formation of the collapsed

https://dx.doi.org/10.1021/acsnano.9b08984
ACS Nano XXXX, XXX, XXX−XXX

structure.[22,23] The mechanism of collapse also depends on the elasticity and cohesiveness of the monolayer.[24] Previous reports with relevance to this study have shown that whiskey inherently contains chemicals that facilitate the generation of interfacial monolayers,[25] and dilution of whiskey with water facilitates the transport of chemicals to the interface.[26]

American whiskey is a spirit distilled at less than 95% alcohol by volume (ABV) from a fermented mash of grain and is bottled at no less than 40% ABV.[27] Various forms of American whiskey exist (*i.e.*, bourbon whiskey, rye whiskey, wheat whiskey, *etc.*) with the defining characteristic being the mixture of grains used in the mashing process.[28] During fermentation, secondary products, known as congeners, are formed by side reactions and determine most of the organoleptic qualities of the final product. The congeners include phenols, aromatics, esters, aldehydes, higher alcohols, and trace substances.[29] After distillation, the product could be stored in a charred new oak barrel for at least two years but is typically stored for four years or longer. During the storage period, complex wood constituents are extracted by the liquid, and reactions occur between various organic substances, resulting in maturation of the product. Maturation of whiskey increases the concentration of acids, esters, and dissolved solids.[30,31] American whiskey differentiates itself from other whiskeys in that maturation occurs in new charred oak containers. The amount of solids contained in American whiskey is greater than whiskeys aged in reused containers (1.8 g/L for straight bourbon whiskey compared to 0.97 g/L for Canadian whiskeys and 1.27 for Scotch).[32] Whiskeys derived from new charred oak barrels have relatively larger concentrations of water-insoluble content.[31] Further, bourbon whiskey has typically been described as more resinous compared to other whiskeys, with the foam from the former being more oily and remaining much longer than that in the latter.[31]

Many of the organic components contained in whiskey are amphipathic and alcohol-soluble.[26] The dilution of a whiskey with water results in the aggregation of the amphipathic molecules into nanoscale agglomerates. This can be demonstrated by diluting the whiskey with water, while stirring the solution and shining a laser through the side of the container (Figure 2). Due to the Tyndall effect,[33] the scattered light from the laser is brightest at a dilution of 20–30% ABV, where agglomerates are largest in size and/or concentration. This visualization effect is reduced at higher alcohol concentrations due to the alcohol-soluble nature of the constituents. These qualitative observations guided droplet evaporation experiments, which were conducted at 20–25% ABV.

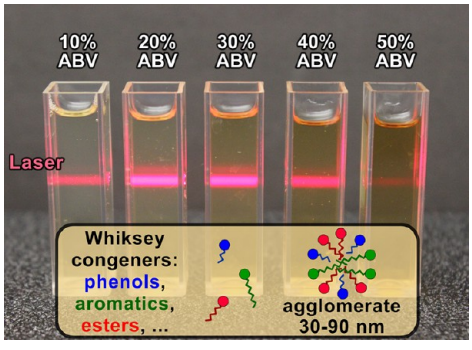

Figure 2. Emergence of colloidal systems in diluted whiskeys. Demonstration of the Tyndall effect, where a laser beam visualizes the suspended agglomerates in various dilutions of a bourbon whiskey.

RESULTS AND DISCUSSION

First, we investigated whether such structures deposited on the substrate or formed on the liquid–air interface. A time-lapse of monolayer formation visualized with dark-field phase contrast is shown in Figure 3 (with an accompanying Movie S1,

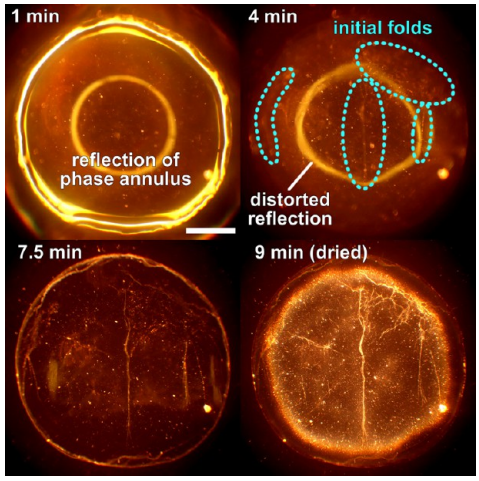

Figure 3. Time-lapse of a 0.75 μL drop of diluted (25% ABV) bourbon whiskey evaporating on the surface of an ITO-coated glass slide under ambient conditions. Evaporation is observed with an upright microscope using a dark-field phase annulus. At 4 min, monolayer folds were observed that subsequently impact the topography of the droplet. Additional folds were created as the droplet evaporates (7.5 min), and these features are highlighted once the liquid has completely evaporated (9 min). Scale bar is 0.5 mm

Supporting Information). Through manual focus adjustment, it was confirmed that the structures were at the liquid–air interface, suggestive of monolayer formation and collapse. The initial image (Figure 3, 1 min) was relatively axisymmetric, evidence of the circular reflection of the phase annulus. However, the reflection became distorted as the monolayer collapsed (Figure 3, 4 min). The monolayer continued to collapse across the droplet surface area, and these features were more clearly visible once the fluid completely evaporated (Figure 3, 9 min).

A side-view time-lapse showing the evaporation of a diluted bourbon whiskey drop is shown in Figure 4, confirming interfacial distortion during evaporation. During evaporation, the monolayer was exposed to stress due to the decreasing surface area, eventually causing it to collapse when exposed to a surface pressure greater than the equilibrium spreading pressure.[22] The overlapping of microcrystalline, inhomogeneous textures occurs during continuous overcompression.[21] Assuming a spherical cap and a base diameter of 2.0 mm, the surface area of a 1.0 μL pinned droplet will reduce by approximately 33% during evaporation. Further, the presence of a rigid monolayer will disrupt sessile evaporation,[34] including significantly reducing the rate of evaporation.[35,36]

Figure 5 illustrates how whiskey web structures were created. First, when a droplet of a diluted whiskey is initially placed onto the substrate, agglomerates are driven to the surface of the droplet through solutal Marangoni flows[37] characterized by

https://dx.doi.org/10.1021/acsnano.9b08984
ACS Nano XXXX, XXX, XXX–XXX

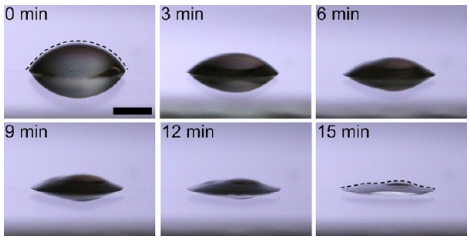

Figure 4. Series of images illustrating the evaporation of 2.5 μL drop of diluted (25% ABV) bourbon whiskey on the surface of an ITO-coated glass slide under ambient conditions. A distorted (*i.e.*, nonaxisymmetric) surface profile is observed, suggesting inhomogeneous mechanical properties at the liquid–air interface. Scale bar is 1.0 mm. Refer to Table S1 in the Supporting Information for sample identification.

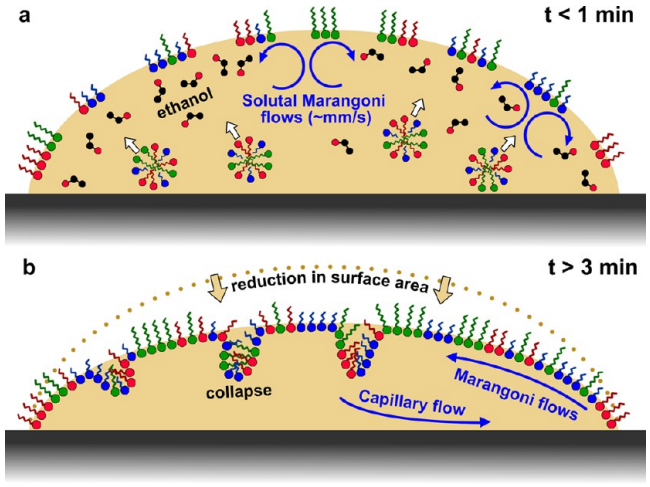

Figure 5. Schematic of the two general phases of flow and monolayer self-assembly observed during whiskey web assembly. (a) First phase is characterized by erratic solutal Marangoni vortices as ethanol is driven to the liquid–air interface, influencing monolayer formation and composition. (b) Monolayer collapse occurs during bulk evaporation as the interfacial area of the droplet decreases and was first observed approximately 3 min into droplet evaporation. Significantly reduced radial flows were observed.

volatile and erratic vortices[38] (Figure 5a). As the concentration of ethanol is greater closer to the interface because of the lower surface tension of ethanol,[39] the transport of ethanol toward the interface also drives water-insoluble chemicals toward the surface,[26] where they disperse into monolayers.[40] To visualize bulk fluid motion, fluorescent microparticles (0.52 μm) were added to the sample and observed during evaporation of the droplet (Movie S2, Supporting Information). Vortices occur during the first phase of bulk volatile evaporation and are typical for ethanol–water droplet evaporation.[38] The second phase of evaporation is characterized by a more subdued radial bulk flow, governed by thermal and surfactant-driven Marangoni stresses (Figure 5b).

Figure 6 shows the multiple length scales associated with these self-assembled structures, where square millimeter films were generated from micrometer strands of nanometer-thick monolayers. The collapsed monolayers (see the scanning electron microscope (SEM) image in Figure 6 and additional SEM images in Figure S1, Supporting Information) have a strong resemblance to a traditional "twisted ribbon" fold.[41]

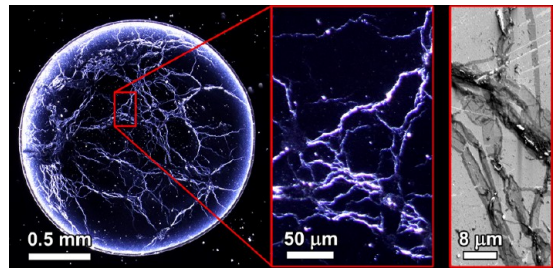

Figure 6. Magnification of the whiskey web structures. SEM imaging of the whiskey web shows the distinct folds of these structures (additional SEM structures are available in Figure S1, Supporting Information).

Although folded monolayers were clearly visible using dark-field and/or light scattering techniques, confirming the presence of uncollapsed monolayers presents a greater challenge. We used energy-dispersive X-ray spectroscopy (EDS) for elemental analysis of whiskey evaporated on ITO-coated glass slides (Figure S2, Supporting Information). There were elevated levels of carbon at the site of collapse (20% normalized mass) and at uncollapsed sizes (3.5%) relative to a plain ITO slide (0.4%), inferring that organic compounds from the whiskey were deposited on the surface of ITO and with greater concentrations at fold sites.

Intuitively, one would expect that the density of collapsed structures would increase with more hydrophobic surfaces as a larger droplet confined over smaller liquid–solid area will result in a denser material network deposit. Figure S3 (Supporting Information) does indeed demonstrate this trend when diluted whiskey droplets of larger volumes (2.0, 5.0, and 10.0 μL) were deposited in a polytetrafluoroethylene (PTFE)-printed slide with fixed 2.0 mm wells. Further, droplets of less than 0.5 μL did not create collapsed monolayers (data not shown). Even though the density of collapsed structures increased with larger droplet volumes, the distinct "chemical fingerprints" (Figure 1) of each brand became comparatively less distinctive and more challenging to qualitatively differentiate.

Particle image velocimetry measurements during the first phase of evaporation were conducted to explore whether or not fluid dynamics induced monolayer collapse. Previous work studying evaporation of undiluted Scotch droplets[10] measured fluid vortices on the order of 100 μm/s, whereas our diluted American whiskey samples reached velocities in excess of 10 mm/s (Figure S4, Supporting Information). The estimated shear stress, τ, associated with this flow was compared to the collapse pressure of the monolayer, evaluated as

$$\tau \approx \mu \frac{\Delta u}{\Delta h} = \gamma / L$$

where μ is viscosity (1 mPa·s), u is velocity (10 mm/s), h is the average height of the droplet (100 μm), γ is the collapse pressure (on the order of 10 mN/m), and L is the length scale of the droplet (1 mm). The fluid shear stress was calculated to be on the order of 100 mPa, which was not enough to overcome the collapse pressure of monolayers (calculated to be 10 Pa for these parameters). Even though fluid shear may not directly induce monolayer collapse, it likely plays a role in the transport of compounds during heterogeneous monolayer formation or surface patterning.[42]

https://dx.doi.org/10.1021/acsnano.9b08984
ACS Nano XXXX, XXX, XXX–XXX

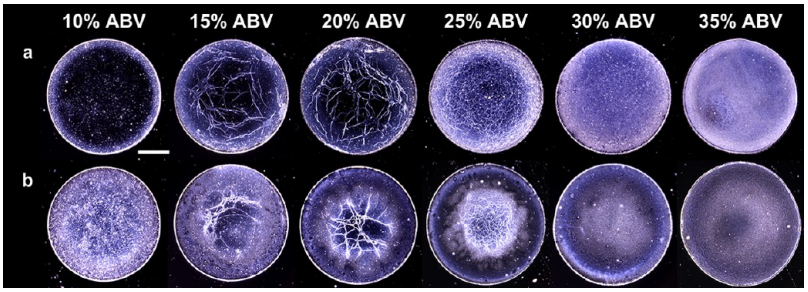

Figure 7. Effect of dilution on the deposited whiskey webs. Web formation of various aged samples: (a) 3 years old and (b) 23 years old. Scale bar is 0.5 mm. Refer to Table S1 in the Supporting Information for sample identification.

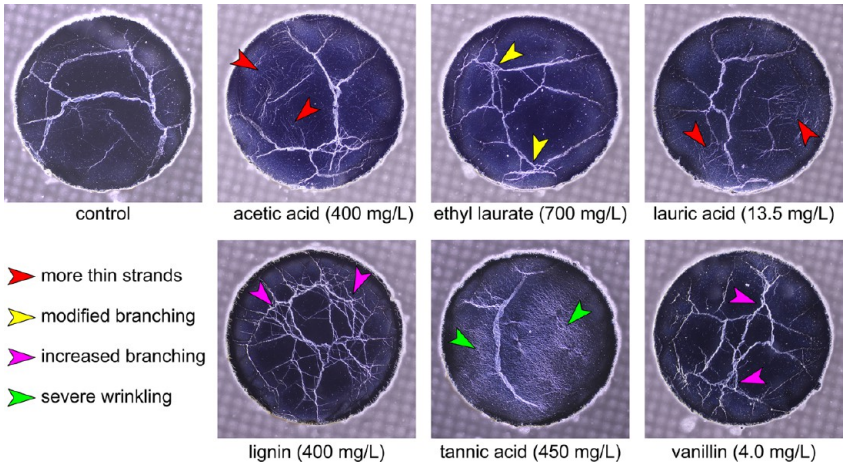

Figure 8. Effect of a set of model congeners on whiskey web patterns. Various congeners were added to a control bourbon whiskey to demonstrate that the concentration and combination of these compounds ultimately guide each whiskey web pattern.

Whiskey web formation was a function of dilution for similar sized droplets (Figure 7). In general, whiskey webs formed when various American whiskey samples were diluted within a specific range, approximately 15−25% ABV. At alcohol concentrations lower than 10% ABV, most whiskey samples deposited in a simple coffee ring pattern (Figure 7a, 10% ABV). However, longer-aged American whiskeys did not exhibit the coffee ring effect at lower alcohol concentrations (Figure 7b, 10% ABV). Elevated levels of solutes, including surfactants, occur in longer-aged samples, and the relatively high surfactant concentration may prevent the formation of a coffee ring.[43] At alcohol concentrations greater than 25%, the samples deposited a nearly uniform film (Figure 7, 30−35% ABV), similarly to previous studies with Scotch.[10] Several factors may contribute to the absence of monolayer collapse at elevated ethanol levels. First, as the ethanol concentration increases, chemical constituents become more soluble and the monolayer becomes more mobile, reducing the occurrences of collapse[44] or, perhaps, alternatively facilitating the formation of vesicles. Second, once the ethanol evaporates and the monolayer is established on the remaining aqueous volume, a greater ABV results in a smaller reduction in the aqueous surface area, thereby lowering the incidence of collapse. Third, previous investigations into chemical activity in the whiskey's headspace demonstrated that a higher concentration of agglomerates reduces volatility;[45−47] therefore, a lower dilution (*i.e.*, higher ABV) will reduce the magnitude and duration of the solutal Marangoni flows that impact the initialization of the monolayer itself. The data in Figure 7 show that whiskey web formation occurs for a specific combination of chemical constituents and ethanol concentration.

Oscillating pendant drop tests were conducted to measure the surface viscoelasticity of whiskey, which provides insight into the presence of surface-active molecules at the liquid−air interface. Figure S5 shows the surface tension response to surface area oscillations for bourbon whiskey and unaged whiskey each diluted to 25% ABV and 15% ABV. Surprisingly, data indicated that only the 15% ABV bourbon whiskey sample showed measurable change in surface tension, suggesting the presence of surfactant molecules at the interface. These data can be explained by the hypotheses that bourbon whiskey surfactants were solubilized in the bulk and/or the rigidity of the monolayer was reduced at elevated ethanol concentrations (25% ABV) compared to reduced levels (15% ABV). Second, these measurements show that whiskey maturation results in the generation of chemical constituents that are strongly surface-active in monolayer formation.

Thousands of chemicals are found in whiskeys, and many of them may contribute toward the molecular assembly of the collapsed monolayers described herein. The unique concentration and combination of congeners that comprise each American whiskey's flavor profile ultimately guide their correspondingly distinctive whiskey web patterns (Figure 1). To further demonstrate this, a control bourbon whiskey was spiked with one of several key constituents that have been identified in whiskeys: acetic acid (400 mg/mL), ethyl laurate (700 mg/mL), lauric acid (13.5 mg/mL), lignin (400 mg/mL), tannic acid (450 mg/mL), and vanillin (4.0 mg/mL). These concentrations were selected to represent the mean level

https://dx.doi.org/10.1021/acsnano.9b08984
ACS Nano XXXX, XXX, XXX−XXX

of each respective chemical or represent that of their collective chemical group (*e.g.*, ethyl laurate for fatty acid ethyl esters), typically found in whiskeys.[48] Figure 8 shows that each congener influences the structure of a formed whiskey web in a specific way. However, predicting how every congener within whiskey will influence monolayer collapse is nontrivial. The collapse behavior of chemically homogeneous monolayers does not correlate with the response of heterogeneous monolayers.[18] Also, the presence of agglomerates, particles, and impurities may result in lower than expected collapse pressures.[22,49] A thorough experimental approach is likely needed to determine the influence of a particular combination of congeners in monolayer formation and collapse. For example, we demonstrated that similar structures can be created from a 1.0 μL droplet of 50% ABV of 1.0 mg/mL lauric acid and 1.5 mg/mL tannic acid (Figure S6, Supporting Information); the future methodical experimental manipulation of relative concentrations will provide insight into their heterogeneous performance.

Most of the tested American whiskeys (65 of 66 samples, refer to Table S1, Supporting Information) formed webs when drying 1.0 μL droplets at 25% ABV. The distinctive visual features of the evaporated structures were generally repeatable from the same bottle of American whiskey. Even the least aged available sample, which was matured for 3 months, produced a whiskey web. However, unaged distillates at the same dilution (n = 5) did not form webs nor uniform films (Figure S7a, Supporting Information). The lack of web structures for unaged whiskey indicates that the components extracted during the aging process are needed to form whiskey webs.

The following aggregated image pattern identification test was conducted to evaluate the repeatability of evaporated whiskey web patterns and to demonstrate how digital image analysis could be used for identification. Three different American whiskeys from the same distiller were selected, and 30 web images were acquired for each sample (90 total). For a given whiskey, 25 images were analyzed and averaged to represent that sample's digital "fingerprint". Next, the remaining 15 images (five of each sample) were compared to each of the three samples' "fingerprint". The individual images were matched correctly over 90% of the time, thus demonstrating the repeatability of whiskey web formation. In the future, the identification process can be strongly enhanced by using machine learning digital algorithms for shape matching and structure identification.[50,51] However, it is important to note that we observed that environmental conditions (temperature, humidity, *etc.*) would impact web formation, and as such, their impact on monolayer integrity should be considered.

The only American whiskey sample tested that did not form webs had been aged 42 years and likely contained elevated levels of surface-active compounds. The presence of the surfactant itself could disrupt the rigidity of the monolayer, resulting in a more mobile layer that is less likely to buckle. To demonstrate that elevated levels of common surfactant suppress web formation, 0.005 wt % of sodium dodecyl sulfate (Sigma-Aldrich, USA) was added to a control sample that otherwise formed webs—this resulted in the formation of a uniform film void of web structures.

The influence of maturation-derived surfactants on the final self-assembled pattern may also be evident in older-aged samples. This is illustrated in Figure 1g,i,j,m, showing samples which were aged at least 15 years. Compared to most of the other images in Figure 1, these have reduced or nonexistent collapsed structures near the perimeter of the droplet. As the droplet evaporates, surfactants tend to have an increased concentration near the perimeter of the droplet. The relative increase in surfactant concentration at the perimeter may result in less rigid monolayers closer to the droplet's edge, thereby reducing the incidence of collapse near the perimeter.

Interestingly, webs did not form under the same conditions for diluted 1.0 μL drops of non-American whiskeys such as Scotch, brandy, Irish whiskey, *etc.* (Figure S7b,c and Table S1, Supporting Information). These products are distilled from different mashes with various finishing processes ranging from the addition of coloring to aging in uncharred new oak barrels or used charred oak barrels.[29] Recall that whiskeys derived from new charred oak barrels have greater solids content[32] and relatively larger concentrations of water-insoluble content.[31] Therefore, the reduced overall concentration of solutes, including water-insoluble components, is likely why monolayer collapse was not observed under similar conditions (20−25% ABV, 1.0 μL). However, we did find that two non-American whiskeys produced self-assembled structures with a greater droplet volume (2.0 μL) and lower dilution (40% ABV); refer to Figure S8, Supporting Information.

CONCLUSIONS

In summary, the results reported here show that whiskeys are chemically complex liquids whose chemical profiles not only distinguish each product[52] but are also responsible for the uniqueness of each product-specific pattern of deposits from drying droplets. Our findings strongly suggest that the new charred barrels have components that readily dissolve in ethanol, which form colloidal suspensions when diluted with water due to nanoparticle precipitation or solubilization (though this is not the only alcoholic spirit that forms colloids with water dilution).[53] These constituents derived from new barrel maturation are critical to whiskey web formation. Further, it may be possible to form these structures using samples other than American whiskeys under conditions that exacerbate web formation including solutions that encompass greater levels of similar colloids and/or evaporation on more hydrophobic surfaces (*i.e.*, greater change in surface area during evaporation).

One unexpected and visually impressive finding is that congeners, comprising less than 1% (by weight) of whiskey composition, are responsible for the creation of self-assembled structures that span several length scales, beginning with the collapse of sub-micrometer monolayers from nanoscale agglomerates to the final weblike structure that covers several square millimeters. Use of digital image analysis may enable visual identification of the product and degree of (desired or not) dilution. For example, web patterns become less dense with increasing dilution (Figure 7, 15−25% ABV), and a straightforward digital image analysis tool can be used to identify adulterated whiskey. To this end, we assembled a simple smartphone-based visualization platform (Figure S9, Supporting Information), enabling portable acquisition of whiskey web digital images. Our preliminary data show that such digital image inspection may lead to simple chemical analysis of American whiskeys; furthermore, this simple and surprisingly distinctive effect may be applicable to similar characterization of spirits[54] or other volatile liquids.

https://dx.doi.org/10.1021/acsnano.9b08984
ACS Nano XXXX, XXX, XXX−XXX

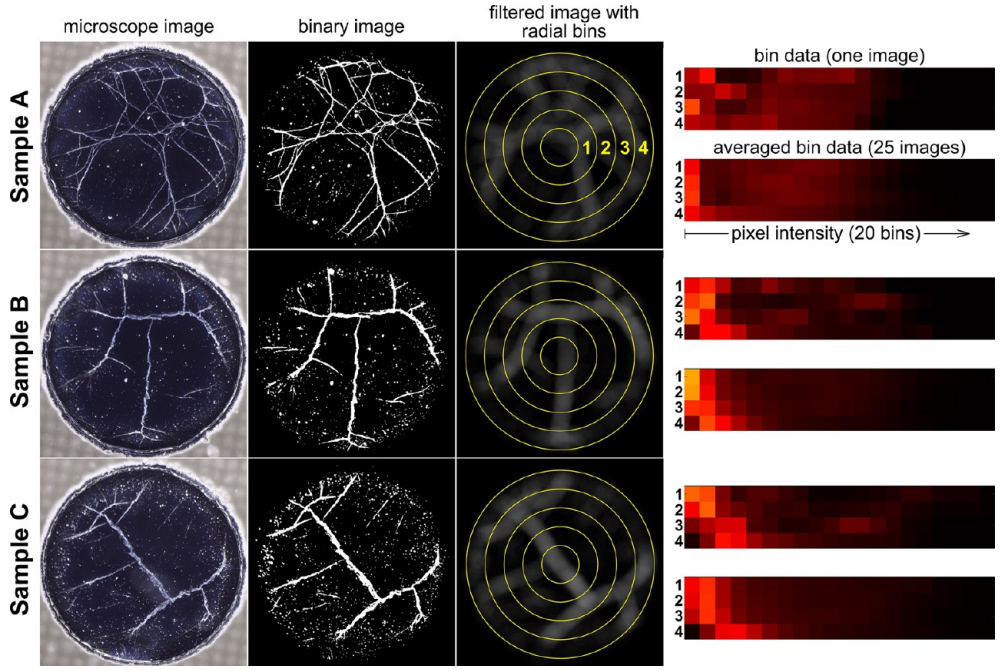

Figure 9. Analysis of microscope images of web patterns. Thirty droplets of each tested American whiskey sample were imaged and analyzed. Digital images were converted to binary images and processed with a radial filter. Each pixel was then placed into a bin based on their radial position (four bins) and intensity (20 bins). Twenty-five arrays were averaged to represent a given American whiskey sample. The remaining 15 droplets (five of each sample) were tested against the averaged representative data. A single image was matched with its American whiskey over 90% of the time. Refer to Table S1 in the Supporting Information for sample identification.

METHODS

Three different substrates were used for the evaporation of droplets: PTFE-printed slides containing 30 2.0 mm wells (Electron Microscopy Science, #63434-02, Hatfield, PA), microscope cover glass (22 × 50 mm, VWR, #16004-314, Radnor, PA), and indium tin oxide (ITO) glass slides (SPI Supplies, West Chester, PA). The latter were used exclusively for SEM images and EDS analysis. Substrates were submerged in a sonicated acetone bath for at least five minutes prior to testing.

Whiskey samples (Table S1, Supporting Information) were either acquired through commercial purchase, generously donated by colleagues, or provided by the distiller. Whiskey samples were diluted with deionized water and mixed prior to droplet deposition. Evaporation occurred under ambient conditions (20−22 °C, 30−46% RH).

Microscopic images were captured using a digital camera (Canon EOS Rebel T7i) mounted to an inverted microscope (Nikon Ti−U) or an upright microscope (Zeiss Axio Imager). For the inverted microscope, an LED ring light was mounted above the sample and its height was adjusted for a given microscope objective (2×, 4×, 10×, or 20×) for optimal image contrast. A dark-field phase contrast ring was used in conjunction with the upright microscope. The digital images were not altered except for minor adjustments in contrast levels.

For EDS measurements, Bruker QUANTAX XFlash 6 energy-dispersive X-ray spectroscopy was used with Carl Zeiss SUPRA 35 VP SEM (Bruker Nano GmBH, Berlin, Germany; Carl Zeiss Microscopy, GmBH, 07745 Jena, Germany).

Fluorescent microparticles (1.0 μm, Thermo Scientific Fluoro-max R0100) were added to the diluted whiskey samples for microparticle image velocimetry (similar to that in ref 10), with a final concentration of 0.01% solids. A 25% ABV 1.0 μL droplet sample was deposited on a cleaned PTFE-printed slide. Image pairs (Δt = 1.4 ms) were acquired every 0.24 s with a high-speed camera (HiSpec 4, Fastec Imaging) mounted to an inverted microscope (Nikon Ti−U, 4× objective with 0.13 NA). Particles were illuminated with scattered light using an LED ring light.

Interfacial rheology was conducted *via* the pendant drop technique using a Ramé-Hart goniometer. Bourbon whiskey and unaged whiskey were diluted with deionized water to 25 and 15% ABV. Liquid droplets of approximately 8 μL were dispensed into a sealed cuvette and surrounded by air. The droplets were then left to rest for up to 30 min. As the droplets aged, evaporation reduced the droplet volume. To compensate for this, small volumes of the liquid were dispensed periodically to maintain a volume of 8 μL. Oscillations were conducted at a frequency of 0.1 Hz and an area displacement ($\Delta A/A_0$) of less than 10% to ensure a mechanical equilibrium between the droplet and the oscillator. Each droplet was oscillated five times to obtain the corresponding change in surface tension. After the oscillation was complete, the droplet was discarded, and a new droplet was formed. This process was repeated in triplicate for each sample, and the results were reported as an average of the three runs.

Congener tests were conducted with acetic acid (Sigma-Aldrich, #A6283), ethyl laurate (Sigma-Aldrich, #W244104), lauric acid (Sigma-Aldrich, #W261408), lignin (TCI America, CAS 8068-05-1), tannic acid (Sigma-Aldrich, #403040), and vanillin (Sigma-Aldrich, #V1104). Congeners were added to a control bourbon whiskey first and mixed before being diluted with deionized water. Two microliter droplets were applied to PTFE-printed slides and evaporated (Figure 4); similar qualitative results were observed for 1.0 μL droplets, but such features were exacerbated using the larger droplet volume.

Three different bourbon whiskeys from the same distiller were selected for repeatability and identification tests (Figure 9). Samples were first diluted to 25% ABV, and then 30 1.0 μL drops of each sample (90 drops total) were evaporated on PTFE-printed slides. Digital images were acquired for each image with an inverted microscope as previously described. A custom MATLAB program was developed for the following analytical procedure. First, digital images (2.4 MP) were converted to a binary image using a threshold function (where black pixels have an intensity value of "0" and white pixels "1"). Next, a circle (of radius R) was fit to each well, and only pixels within this circle were subsequently analyzed (approximately 7.2 million pixels). Next, a circular averaging filter (with filter radius 0.1R) was applied to each binary image to effectively blur the image. The

https://dx.doi.org/10.1021/acsnano.9b08984
ACS Nano XXXX, XXX, XXX−XXX

resulting pixels were then placed into data bins by radius (five bins at equal 0.2R increments) and intensity (20 bins at equal increments across a range of 0 to 0.4). Numerical values of each bin were the percentage of pixels within a certain radial bin found within a specific intensity bin. The first radial bin (0 to 0.2R) was omitted, resulting in a final 4 × 20 data array to represent a single digital web image. A data array was obtained for each of the 90 web images. A second MATLAB program was created in which, for a given whiskey sample of 30 image data arrays, 25 were randomly selected and averaged as a representation of that whiskey sample. The remaining 15 samples (five for each of the three samples) were compared to the three samples' averaged data array using a sum of least squares; the value with the smallest sum was selected as its match. This program was repeated 1000 times and matched individual images successfully over 90% of the time.

Smartphone images were acquired with a clip-on lens (Kingmas 60X) mounted on a Samsung Galaxy Note 8 smartphone.

ASSOCIATED CONTENT

Supporting Information

The Supporting Information is available free of charge at https://pubs.acs.org/doi/10.1021/acsnano.9b08984.

SEM images (Figure S1), EDS analysis (Figure S2), results from a web density study (Figure S3), particle image velocimetry results (Figure S4), oscillating pendant drop results (Figure S5), image of a synthetic weblike pattern (Figure S6), non-American whiskey patterns (Figures S7 and S8), and smartphone visualization (Figure S9) (PDF)

Movie S1 (MP4)

Movie S2 (MP4)

AUTHOR INFORMATION

Corresponding Author

Stuart J. Williams − *Department of Mechanical Engineering, University of Louisville, Louisville, Kentucky 40292, United States;* orcid.org/0000-0002-1678-7544; Email: stuart.williams@louisville.edu

Authors

Adam D. Carrithers − *Department of Mechanical Engineering, University of Louisville, Louisville, Kentucky 40292, United States*

Martin J. Brown, VI − *Department of Mechanical Engineering, University of Louisville, Louisville, Kentucky 40292, United States*

Mohamed Z. Rashed − *Department of Mechanical Engineering, University of Louisville, Louisville, Kentucky 40292, United States*

Sabina Islam − *Department of Chemical and Biomolecular Engineering, North Carolina State University, Raleigh, North Carolina 27606, United States*

Orlin D. Velev − *Department of Chemical and Biomolecular Engineering, North Carolina State University, Raleigh, North Carolina 27606, United States;* orcid.org/0000-0003-0473-8056

Complete contact information is available at: https://pubs.acs.org/10.1021/acsnano.9b08984

Author Contributions

§M.J.B. and A.D.C. contributed equally to this work.

Notes

The authors declare no competing financial interest.

ACKNOWLEDGMENTS

The authors would like to acknowledge those who generously donated samples for this study including E. Downs (Limestone Branch Distillery), T. Effler (Brown-Forman Corp.), P. Heist (Wilderness Trail Distillery), S. Herman (Louisville Metro), J. Kepley (Adaptive Nursing & Healthcare Services), D. Mandell (Bardstown Bourbon Company), C. Miller (Kentucky Artisan Distillery), G. Miller (University of California, Davis), C. Morris (Woodford Reserve Distillery), M. Niemann (Four Roses Distillery), L. Tompkins (University of Louisville), P. Van Winkle (Old Rip Van Winkle Distillery), A.H. Williams (brother of S.J. Williams), C. Zaborowsky (Westport Whiskey & Wine), and K. Zamanian (Rabbit Hole Distillery). The authors greatly appreciate K.A. Erk and C.R. Davis (Purdue University) for performing the pendant drop tests. The authors appreciate valuable scientific conversations with T. Collins (Washington State University) and W. Ristenpart (University of California, Davis).

REFERENCES

(1) Poulard, C.; Damman, P. Control of Spreading and Drying of a Polymer Solution from Marangoni Flows. *Europhys. Lett.* **2007**, *80*, 64001.

(2) Sefiane, K.; Tadrist, L.; Douglas, M. Experimental Study of Evaporating Water-Ethanol Mixture Sessile Drop: Influence of Concentration. *Int. J. Heat Mass Transfer* **2003**, *46*, 4527−4534.

(3) Yunker, P. J.; Still, T.; Lohr, M. A.; Yodh, A. G. Suppression of the Coffee-Ring Effect by Shape-Dependent Capillary Interactions. *Nature* **2011**, *476*, 308−311.

(4) Anyfantakis, M.; Geng, Z.; Morel, M.; Rudiuk, S.; Baigl, D. Modulation of the Coffee-Ring Effect in Particle/Surfactant Mixtures: The Importance of Particle-Interface Interactions. *Langmuir* **2015**, *31*, 4113−4120.

(5) Girard, F.; Antoni, M.; Faure, S.; Steinchen, A. Influence of Heating Temperature and Relative Humidity in the Evaporation of Pinned Droplets. *Colloids Surf., A* **2008**, *323*, 36−49.

(6) Girard, F.; Antoni, M. Influence of Substrate Heating on the Evaporation Dynamics of Pinned Water Droplets. *Langmuir* **2008**, *24*, 11342−11345.

(7) Kuang, M.; Wang, L.; Song, Y. Controllable Printing Droplets for High-Resolution Patterns. *Adv. Mater.* **2014**, *26*, 6950−6958.

(8) Deegan, R. D.; Bakajin, O.; Dupont, T. F.; Huber, G.; Nagel, S. R.; Witten, T. A. Capillary Flow as the Cause of Ring Stains from Dried Liquid Drops. *Nature* **1997**, *389*, 827.

(9) Mampallil, D.; Eral, H. B. A Review on Suppression and Utilization of the Coffee-Ring Effect. *Adv. Colloid Interface Sci.* **2018**, *252*, 38−54.

(10) Kim, H.; Boulogne, F.; Um, E.; Jacobi, I.; Button, E.; Stone, H. A. Controlled Uniform Coating from the Interplay of Marangoni Flows and Surface-Adsorbed Macromolecules. *Phys. Rev. Lett.* **2016**, *116*, 124501.

(11) Williams, S. J.; Brown, M. J.; Carrithers, A. D. Whiskey Webs: Microscale "Fingerprints" of Bourbon Whiskey. *Phys. Rev. Fluids* **2019**, *4*, 100511.

(12) Mohwald, H. Phospholipid and Phospholipid-Protein Monolayers at the Air/Water Interface. *Annu. Rev. Phys. Chem.* **1990**, *41*, 441−476.

(13) Zasadzinski, J. A.; Viswanathan, R.; Madsen, L.; Garnaes, J.; Schwartz, D. K. Langmuir-Blodgett-Films. *Science* **1994**, *263*, 1726−1733.

(14) Phan, M. D.; Lee, J.; Shin, K. Collapsed States of Langmuir Monolayers. *J. Oleo Sci.* **2016**, *65*, 385−397.

(15) Baldelli, S.; Schnitzer, C.; Simonelli, D. Aqueous Solition/Air Interfaces Probed with Sum Frequency Generation Spectroscopy. *J. Phys. Chem. B* **2002**, *106*, 5313−5324.

(16) Liu, J.; Conboy, J. C. Phase Transition of a Single Lipid Bilayer Measured by Sum-Frequency Vibrational Spectroscopy. *J. Am. Chem. Soc.* **2004**, *126*, 8894−8895.
(17) McConnell, H. M. Structures and Transitions in Lipid Monolayers at the Air-Water-Interface. *Annu. Rev. Phys. Chem.* **1991**, *42*, 171−195.
(18) Carter-Fenk, K. A.; Allen, H. C. Collapse Mechanisms of Nascent and Aged Sea Spray Aerosol Proxy Films. *Atmosphere* **2018**, *9*, 503.
(19) Alonso, C.; Alig, T.; Yoon, J.; Bringezu, F.; Warriner, H.; Zasadzinski, J. A. More Than a Monolayer: Relating Lung Surfactant Structure and Mechanics to Composition. *Biophys. J.* **2004**, *87*, 4188−4202.
(20) Gopal, A.; Lee, K. Y. C. Morphology and Collapse Transitions in Binary Phospholipid Monolayers. *J. Phys. Chem. B* **2001**, *105*, 10348−10354.
(21) Angelova, A.; Vollhardt, D.; Ionov, R. 2D-3D Transformations of Amphiphilic Monolayers Influenced by Intermolecular Interactions: A Brewster Angle Microscopy Study. *J. Phys. Chem.* **1996**, *100*, 10710−10720.
(22) Ybert, C.; Lu, W.; Moller, G.; Knobler, C. M Kinetics of Phase Transitions in Monolayers: Collapse. *J. Phys.: Condens. Matter* **2002**, *14*, 4753−4762.
(23) Lee, K. Y. C. Collapse Mechanisms of Langmuir Monolayers. *Annu. Rev. Phys. Chem.* **2008**, *59*, 771−791.
(24) Lipp, M. M.; Lee, K. Y. C.; Takamoto, D. Y.; Zasadzinski, J. A.; Waring, A. J. Coexistence of Buckled and Flat Monolayers. *Phys. Rev. Lett.* **1998**, *81*, 1650−1653.
(25) Kelly, A. G.; Vega-Mayoral, V.; Boland, J. B.; Coleman, J. N. Whiskey-Phase Exfoliation: Exfoliation and Printing of Nanosheets Using Irish Whiskey. *2D Mater.* **2019**, *6*, 045036.
(26) Karlsson, B. C. G.; Friedman, R. Dilution of Whisky - The Molecular Perspective. *Sci. Rep.* **2017**, *7*, 6489.
(27) Russell, I. *Whisky: Technology, Production and Marketing*; Academic Press: Boston, MA, 2003.
(28) Piggott, J. R.; Sharp, R.; Duncan, R. E. B. *The Science and Technology of Whiskies*; John Wiley & Sons: New York, 1989.
(29) Bujake, J. E. Beverage Spirits, Distilled. *Kirk-Othmer Encyclopedia of Chemical Technology*; John Wiley & Sons: New York, 2007.
(30) Liebmann, A. J.; Rosenblatt, M. Changes in Whisky While Maturing. *Ind. Eng. Chem.* **1943**, *35*, 994−1002.
(31) Crampton, C. A.; Tolman, L. M. A Study of the Changes Taking Place in Whiskey Stored in Wood. *J. Am. Chem. Soc.* **1908**, *30*, 98−136.
(32) Beverage Spirits, Distilled. In *Kirk-Othmer Encyclopedia of Chemical Technology*, 3rd ed.; John Wiley and Sons: New York, 1978; Vol. 3, p 837.
(33) Laidler, K. J.; Meiser, J. H. *Physical Chemistry*; Benjamin/Cummings Pub. Co.: Menlo Park, CA, 1982.
(34) Birdi, K. S. *Self-Assembly Monolayer Structures of Lipids and Macromolecules at Interfaces*; Kluwer Academic/Plenum Publishers: New York, 1999.
(35) Cheng, A. K. H.; Soolaman, D. M.; Yu, H.-Z. Non-Evaporating″ Microdroplets on Self-Assembled Monolayer Surfaces under Ambient Conditions. *J. Phys. Chem. B* **2007**, *111*, 7561−7566.
(36) Mansfield, W. W.; Mysels, K. J.; Wu, J. Evaporation Retardation by Monolayers. *Science* **1972**, *176*, 944−945.
(37) Bennacer, R.; Sefiane, K. Vortices, Dissipation and Flow Transition in Volatile Binary Drops. *J. Fluid Mech.* **2014**, *749*, 649−665.
(38) Christy, J. R. E.; Hamamoto, Y.; Sefiane, K. Flow Transition within an Evaporating Binary Mixture Sessile Drop. *Phys. Rev. Lett.* **2011**, *106*, 205701.
(39) Liu, C.; Bonaccurso, E.; Butt, H.-J. Evaporation of Sessile Water/Ethanol Drops in a Controlled Environment. *Phys. Chem. Chem. Phys.* **2008**, *10*, 7150−7157.
(40) Ries, H. E. Heart-Shaped Monolayer Islands and Ridged Collapse Structures of Ceramide Galactoside. *J. Colloid Interface Sci.* **1982**, *88*, 298−301.
(41) Ries, H. E.; Swift, H. Twisted Double-Layer Ribbons and the Mechanism for Monolayer Collapse. *Langmuir* **1987**, *3*, 853−855.
(42) Bassou, N.; Rharbi, Y. Role of Benard-Marangoni Instabilities during Solvent Evaporation in Polymer Surface Corrugations. *Langmuir* **2009**, *25*, 624−32.
(43) Hu, H.; Larson, R. G. Analysis of the Effects of Marangoni Stresses on the Microflow in an Evaporating Sessile Droplet. *Langmuir* **2005**, *21*, 3972−3980.
(44) Bhamla, M. S.; Chai, C.; Alvarez-Valenzuela, M. A.; Tajuelo, J.; Fuller, G. G. Interfacial Mechanisms for Stability of Surfactant-Laden Films. *PLoS One* **2017**, *12*, e0175753.
(45) Piggott, J. R.; Gonzalez Vinas, M. A.; Conner, J. M.; Withers, S. J.; Paterson, A. Effect of Chill Filtration on Whisky Composition and Headspace. In *Flavour Science: Recent Developments*; Taylor, A. J., Mottram, D. S., Eds.; Woodhead Publisher: Cambridge, U.K., 1997.
(46) Conner, J. M.; Piggott, J. R.; Paterson, A.; Withers, S. Interactions between Wood and Distillate Components in Matured Scotch Whisky. In *Flavour Science: Recent Developments*; Taylor, A. J., Mottram, D. S., Eds.; Woodhead Publisher: Cambridge, U.K., 1997.
(47) Boothroyd, E. L.; Linforth, R. S. T.; Cook, D. J. Effects of Ethanol and Long-Chain Ethyl Ester Concentrations on Volatile Partitioning in a Whisky Model System. *J. Agric. Food Chem.* **2012**, *60*, 9959−9966.
(48) Freitas, R. A. *Whiskey Machine: Nanofactory-Based Replication of Fine Spirits and Other Alcohol-Based Beverages*; http://www.imm.org/Reports/rep047.pdf (accessed 2020-02-26).
(49) Kuo, C.-C.; Kodama, A. T.; Boatwright, T.; Dennin, M. Particle Size Effects on Collapse in Monolayers. *Langmuir* **2012**, *28*, 13976−13983.
(50) Reinhart, W. F.; Long, A. W.; Howard, M. P.; Ferguson, A. L.; Panagiotopoulos, A. Z. Machine Learning for Autonomous Crystal Structure Identification. *Soft Matter* **2017**, *13*, 4733−4745.
(51) Phillips, C. L.; Voth, G. A. Discovering Crystals Using Shape Matching and Machine Learning. *Soft Matter* **2013**, *9*, 8552−8568.
(52) Collins, T. S.; Zweigenbaum, J.; Ebeler, S. E. Profiling of Nonvolatiles in Whiskeys Using Ultra High Pressure Liquid Chromatography Quadrupole Time-of-Flight Mass Spectrometry (UHPLC-QTOF MS). *Food Chem.* **2014**, *163*, 186−196.
(53) Vitale, S. A.; Katz, J. L. Liquid Droplet Dispersions Formed by Homogeneous Liquid-Liquid Nucleation: ″The Ouzo Effect. *Langmuir* **2003**, *19*, 4105−4110.
(54) Gonzalez-Gutierrez, J.; Perez-Isidoro, R.; Ruiz-Suarez, J. C. A Technique Based on Droplet Evaporation to Recognize Alcoholic Drinks. *Rev. Sci. Instrum.* **2017**, *88*, 074101.

https://dx.doi.org/10.1021/acsnano.9b08984
ACS Nano XXXX, XXX, XXX−XXX